EMERGING MINDS
JOURNAL FOR STUDENT RESEARCH

ISSN 2976 - 9094
EMJSR 2024, Vol. 2 (1): 13-39
https://doi.org/10.59973/emjsr.48

Received: 2024-09-01
Accepted: 2024-26-01
Published: 2024-04-02

Multi-Colour Photometric Observations of Transiting Exoplanets to Verify Binary Star Systems

Thomas Franklin [1*]

[1] University of Portsmouth, School of Mathematics and Physics, Portsmouth, PO1 3FX, United Kingdom
*Corresponding author (Email: tf1.franklin@gmail.com)

Abstract – Within this paper, we report the observation of transiting exoplanets, K2-29b, TrES-3b, WASP-36b, and HAT-P54b, with a focused comparison of the well-defined binary system K2-29b to the proposed binary WASP-36b. Performing multicolour photometry, debayering images to three distinct colour channels, a comparison of the detrended light curves of each target is used to define parameters to identify the presence of any discrepancy between the observation, defined system models or past observations. The exoplanet system K2-29b, observed in separate red and blue filters, produced minimal deviation from expected R_P/R_* values with $R_P/R_* = 0.1404^{+0.0040}$ and $R_P/R_* = 0.1468^{+0.0082}$ respectively. In contrast to this, we observe a significant deviation in the blue debayered value of R_P/R_* for WASP-36b, with the expected radius ratio defined to be $R_P/R_* = 0.1368$ 0.0006. Initial airmass detrending model fitting for the blue debayered channel produced a value of $R_P/R_* = 0.1162^{+0.0098}$, with R_P/R_* Drift = 3.01σ, this later being reduced through a quadratic detrending scheme to R_P/R_* Drift = 2.11σ. Despite this model being an improved representation, this measure of R_P/R_* drift is significantly beyond the tolerance of 1σ and as such motivates further study as this effect has been denoted in concordant research to suggest presence of a secondary star in this system.

Keywords – Exoplanet, Binary star systems - *Methods*: Observational, Ground based, Transit - *Techniques*: Photometry, HOPS.

1. Introduction

Ground-based observations of extrasolar planets allow astronomers to gain valuable insights into the properties which govern these distant systems. The primary objective in this research is to assess the viability of one detection method, multicolour photometry of an exoplanet's transit [N1], to verify the planet's existence or reinforce observational data to improve its model parameters. While observations from within Earth's atmosphere may present limitations, techniques to reduce systematic and random errors continue to demonstrate the worth of this cost-effective method for proposed exoplanet validation. Given analysis of Transiting Exoplanet Survey Satellite (TESS) targets over time, it is suggested that measurements within a year from its last observation may incur errors of up to 30 minutes [1]. 2019). As such, this research aims to contribute to the ESA Atmospheric Remote-sensing Infrared Exoplanet Large-survey (ARIEL) mission by reducing ephemerid errors, as well as identifying any presence of any false positive detections often recorded by wide field surveys such as TESS [2]. Additionally, to optimise future use of the ARIEL observation timings [3], particularly for complex systems, all results presented within Section 4 and Appendix A, B, C, D shall offer supportive data for the Ariel mission through the consortium project, ExoClock, to ensure measurement and report requirements, constructing statistical models from the vast exoplanet detection and verification of both professional and amateur astronomers. Continual verification of target location and dynamics performed using ground-based observational techniques, such as Radial Velocity (RV), gravitational lensing, and astrometry, alongside transits, enable the success of advanced research, such as the James Webb Space Telescope (JWST), which is providing an understanding of exoplanetary atmospheric dynamics, composition, and confirming their physical parameters with greater precision [4].

This paper explores the application of the transit method to update the parameters which describe such exoplanets, with emphasis on dictating the likelihood of a correlation between the behaviour of complex star systems, which may lead to observed phenomena such as Transit Timing Variation (TTV) or differences in measured flux, or radius radio drift. Through observation of hot Jupiters [N2], we have selected suitable targets for analysis featuring visible transits within the project duration using the research-grade scientific equipment at Clanfield Observatory. Measuring deviation

in radius or transit duration from prior definition of system parameters allows exploration of such a relationship between the presence of stellar companions with residuals measurement.

2. Theory

2.1 The Radius Ratio

When a planet's orbital plane aligns with our visual axis (impact parameter [N3], $b = 0.0$) we observe a dip in the star's apparent brightness as the planet appears to move across it, derived within Appendix: E.1. From this relationship, we can deduce the planet's size without the need for direct imaging which would not be possible for many targets which can be observed from hundreds to thousands of light years from Earth. Equation 1 outlines this relationship where the ratio between exoplanetary and stellar radius, R_P/R_*, can be equated to the proportion of flux, ΔF, lost compared to before transit.

$$\frac{\Delta F}{F} = \left(\frac{R_P}{R_*}\right)^2 \tag{1}$$

This integral method for estimating exoplanet size holds for all interstellar transits where it passes, in totality, the visible two-dimensional 'photosphere' surface area which itself, in this idealised case, possesses no limb darkening [N4]. The presence of limb darkening can be observed in the light curve as a smoothly varying dip after steep ingress or before steep egress, see Figure 2, and in such cases fitting of a limb darkening coefficient model's intensity profile is not directly comparable to the fitting of a light curve. Because of this, the selection of nonlinear laws to directly obtain Limb Darkening Coefficient (LDC) quantities develops these with repeated observations over time, where strict requirements form a representative compensation for the given system [5 – 8]. Similar to the influence caused by Rayleigh scattering where blue wavelengths exhibit increased apparent R_P [9], this wavelength-dependant effect strengthens the motivation to employ multicolour photometry as a method to identify the curvature dependence of the transit line's base to select wavebands which best identify transit phases. s which best identify transit phases.

2.2 Transit Duration

Thus far we have presumed no influence of impact parameter, but in observations, this quantity is rarely nonzero. Through use of some trivial assumptions and trigonometry, we can produce accurate approximations of observed transit descriptors including orbital inclination, i, and semi-major axis, a, which in many cases is approximated to near zero. These quantities are then evaluated with light curve's shape, confirming a suitable result for transit duration and radius ratio between the aforementioned ingress or egress.

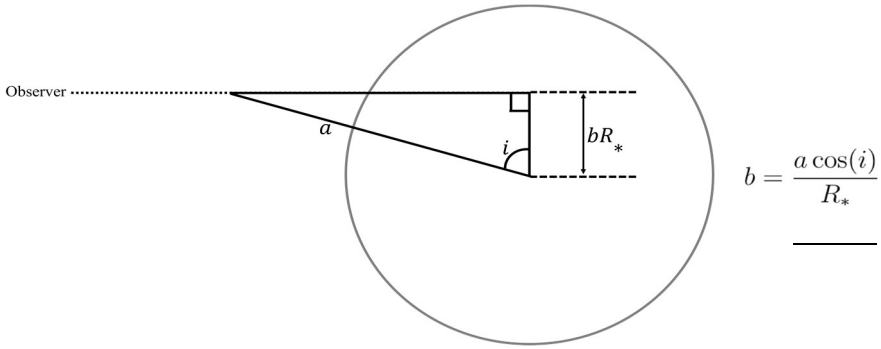

Figure 1. Diagram defining the impact parameter b as a proportion of the stellar radius relative to the Observer's point of view. (*Left*); Equation for Impact Parameter (*Right*).

Further to this, we can now define the duration of the transit mathematically, given its dependence on Equation 2.2, where the greater this offset, the shorter the duration we observe. The details of this derivation are well defined and can be found detailed within, [10,11], and Appendix E.2 to describe the fraction of a full orbital period, P, under the assumption that $R_P << R_*$.

$$T_{dur} = \frac{P}{\pi}\sin^{-1}\left(\frac{\sqrt{(R_P + R_*)^2 - b^2}}{a}\right) \tag{3}$$

Despite being an approximation for the circular orbit case, Equation 3 provides a suitable point to further specialise our models based on observation data and RV calculations for orbit eccentricity, *e*. Characterisation through observations across multiple wavelengths incur slightly discordant results, leading to evidence for more complex systems. Such variations as those of TTV can arise through orbital decay by dynamical tidal effects [12], or with the presence of additional bodies. We aim within this work to deduce the potential for a relation between multicolour photometric results of exoplanet transit observations to identify the presence of a stellar binary system about a yet to be classified binary, WASP-36b.

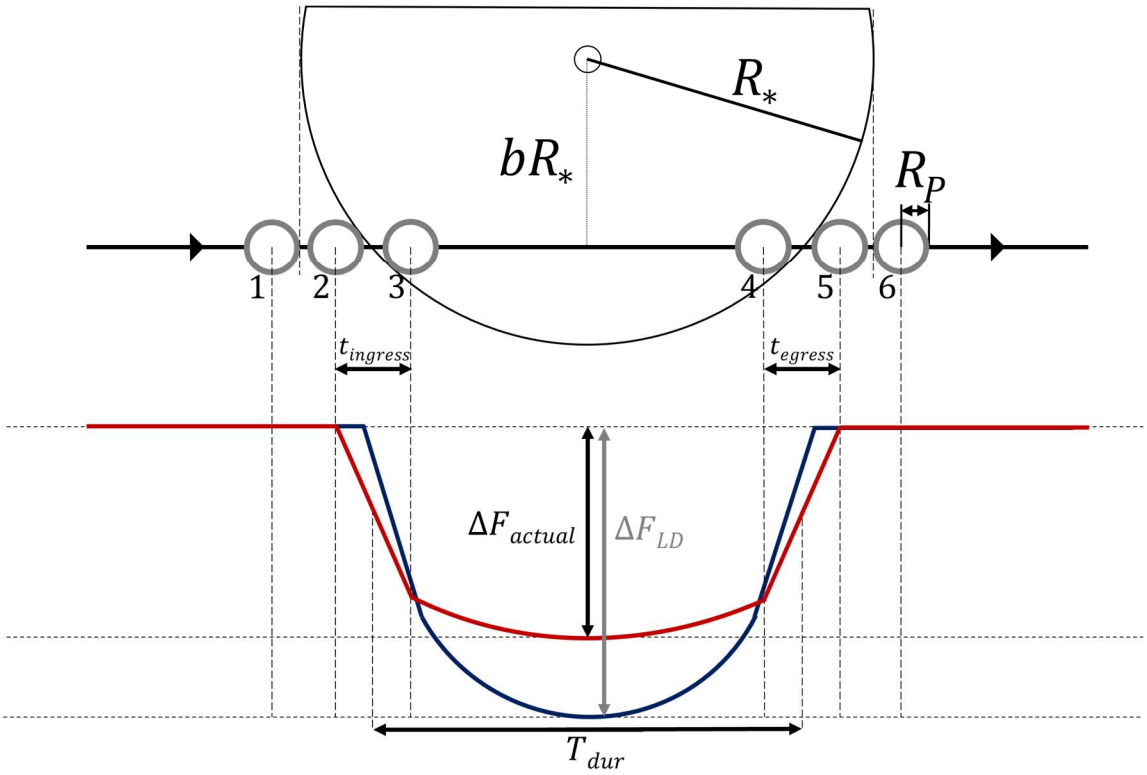

Figure 2. Exoplanet transit with nonzero *b*, where limb darkening changes the near constant R_P/R_* value seen in the red curve to appear more akin to the blue curve, producing a measurement of ΔF which is not representative of the true system. Positions 2-3 represent ingress, 4-5 represent egress, where rate of change of ΔF is greatest.

3. Methodology

3.1 Observation Process

The nature of transit observations presents limitations with low transit probability and commonality of light curve patterns seen across numerous astrophysical phenomena. To ensure effective use of available observation time, targets selected here have well documented RV measurements, and display features which align with transit criterion given the equipment specifications. To provide a deeper characterisation is the motivation for the application of multicolour photometry, assessing features of the obtained light curve [13] which, in conjunction with both transit and alternate observational technique records, enables efficient transit fitting routines for extraction of the accurate physical parameter sets from transit light curves [14].

3.1.1 Target Selection and Observation

The first step for exoplanet observation, once potentially clear conditions have been identified for suitability to perform data collection, is to choose a target. Assessing our observation criteria to match that of the scope used, exoplanet features listed in Table 1, reduced the selection to hot Jupiters which produce a signal suitable for the equipment and displays the greatest recurrence, dominating candidate classification for transiting exoplanets making up over 10% of targets [15]. This selection process took advantage of the Exoclock scheduler, identifying the listed requirements and conditions for observation. Tracking and target identification through Cartes Du Ciel, and Maxim DL software for operation and control of the scientific telescope and cameras at Clanfield observatory, produced continual tracking during several hours over which a transit completes. Once the target is selected and appropriate filters, camera type and scope are chosen, where successful data collection relies upon the correct exposure and in-camera processing

of the images. For a camera with a given bit depth, we can calculate its full well, $2^{BitDepth}$, to correctly set the saturation for the particular environment after initial testing exposures with complete apparatus.
Some preparation for later calibration can also be completed here as binning [N5], while reducing resolution slightly, increases image Signal to Noise Ratio (SNR) due to the counts being summed from each pixel square, $\sum count[i]$, whereas the statistical quantity of read noise when scaling up is the root of the sum of squares $\sqrt{(\sum count[i]^2)}$, producing an image with reduced noise and increased signal in most use cases. Outside of recording the light frames containing sky data for the duration of the transit plus one hour pre-ingress and post-egress for detrending, Section 4.1.1, with collection of dark, bias and flat calibration frames allow for additional calibration and noise reduction, this process discussed further in Appendix G.

Table 1. Clanfield Observatory Telescope Specification for Exoplanet Parameters.

Parameter	24" Scope	16" Scope
Telescope Defined Parameters		
Depth (*mmag*)	>10	>6 R
Magnitude (V_{mag})	<12	>10
Transit Altitude (°)	>30	> 25
Physical Parameters		
Transit Start, Mid, and End Time		
Transit Start, Mid, and End Direction		

Note: Physical parameters vary with target, observation time and lunar cycles.
[a] Quantitative telescope parameter calculated through ExoClock Schedule SNR, where listed values are a guide to flag potential planet-telescope combinations.
[b] Physical parameters dependant on chosen target.

3.1.2 Analysis

Once data collection is complete, analysis and construction of a fitting routine is necessary to compare our observation to expected results as defined in prior research and documentation. If the equipment selected included the use of a multicolour camera with a clear filter, some pre-processing was completed for evaluating the three wavebands recorded by the CMOS. This process is known as 'de-bayering' or 'de-mosaicing', see Appendix G.1.1, G.1.2, G.1.3, where Python script produced as part of this work is also presented. With these frames produced, full analysis of the produced images is conducted through application of the Python-based, HOPS [16], in which a series of analytical steps are followed in order to minimise error and produce the best representative fit of the data collected. As outlined within sources available at [17], this involves target and file identification, reduction of the calibration frames from the light frames, inspection to remove potentially bad frames from use in later analysis, alignment to mitigate Field of View (FOV) deviations during target tracking, photometry of our target star in comparison to selected non-variable stars within the telescope's FOV, before finally running this comparative photometry, and inspecting for any anomalous comparisons before fitting the data to our model.

4. Results and Discussion

4.1 HOPS Result Processing Techniques

4.1.1 Detrending

Compensation for the influence of a trend in the model's residuals, such as the effect of airmass, telescope vibration, or photometry defects, highlight the requirement of a detrending algorithm [18]. This process recognises trends across the duration of the recording time series through a statistical regression analysis through hierarchical tree clustering, to remove the determined trend's effect. This approach to handling results can take different forms depending on the

extent of these values, where in most cases the airmass fit is suitable to account for any gradual minute developments throughout the observation. In some cases, often for more complex systems, additional contributors may influence this, and as such these will require a model with greater adaptability, so a quadratic fitting routine may resolve deviation further from the standard model. In few instances, there may be a linear change in residual value during observation, where a regression line suits such a pattern, leading to a linear detrending approach, however, was not applied to any new results presented in Section 4.3.

4.1.2 Fitting

Selecting the aperture about which a star's photometry is measured over the transit duration can pose challenges as the area of light intensity incident on the sensor may not form perfect point sources about their centre. Because of this, the computational fitting must account for such errors in addition to other non-symmetric properties which negatively impact the model's fitting. This is particularly important in the observation of binary star systems as in some cases we observe the close secondary star to be within this aperture selection of our target; in such a system, each frame should be inspected independently of others by the model, as there is an increased likelihood that resultant calculations will be influenced greatly across the entire transit with this difference.

4.1.3 MCMC

With prior fitting information and statistical calculations to generate certainty in the predicted values from the Root Mean Square (RMS) of the best-fit model's residuals, we can complete the fitting with Markov chain Monte Carlo (MCMC). This Bayesian model constructs an informed light curve prediction from the likelihood and priors dictated by the fitting options in previous steps. This approach for informed model construction improves the interpretation of the numerous features which contribute to the final outcome plotted for Exoclock, displayed in Appendix A.2, B.3, C.1. D.1.

4.2 Transit Variables

While multiple parameters construct a more complete picture of the systems being observed, focus will follow as outlined in Section 2, with comparison of observed-calculated (O-C) and statistical uncertainty the model produced. By doing so, highlighting features of the observations with the potential to suggest the presence of additional bodies orbiting the system, or more poignantly the presence of a secondary star. To assess this, the first observation studies K2-29b, a binary star system using two colour filters before employing the debayering program, Appendix G, to validate suitability of such a routine to convert clear filter images to discrete, multicoloured frames for TrES-3b, HAT-P-54b (Appendix B, D) and finally WASP-36b, the latter being a proposed binary system which we hypothesise will present some deviation from current expected values.

4.3 Transit Targets

4.3.1 K2-29b

As the first of our observations, it was crucial to highlight our ability to image and assess any O-C or expected value deviation from an exoplanet which has been well documented from multiple observation methods. Presented below is a record of two papers which study the system extensively, Table 2, where each paper details some parameters of the system through extensive study and calculation. These results are defined through observations which employed specified use of, r', R, clear, and V filters at apertures ranging from 0.11m-1.04m in [19], with the second being a comparative study of two K2 systems, several methods and bands are stated to contribute to the values, with the final grouping under '*Planet Parameters*' being derived from observation results.

Table 2. Research Paper Results for K2-29b.

Parameter	Detail	M. C. Johnson et al. 2016	Santerne et al. 2016
Orbital Parameters			
P_{orb}	Orbital Period (days)	$3.2589263 \pm 1.5 \times 10^{-6}$	$3.2588321 \pm 1.9 \times 10^{-6}$
$T_{dur} = \tau_{14}$	Transit Duration (days)	0.0887 ± 0.00100	0.0925 ± 0.0004
$\tau_{12} = \tau_{34}$	Ingress/Egress Duration (days)	0.0126 ± 0.0015	-
a/R_*	Scaled Semimajor Axis	11.77 +0.65/- 0.62	10.51 ± 0.15
R_P/R_*	Radius Ratio	0.1373 +0.0024/-0.0026	0.14188 ± 0.00062
δ	Transit Depth (%)	1.884 +0.066/-0.070	-
b	Impact Parameter	0.452 +0.096/-0.15	0.58 ± 0.02
i_p	Orbital Inclination (°)	87.89 +0.75/-0.55	86.656 +0.11/-0.08
a	Semi Major Axis (AU)	0.04097 ± 0.00064	0.04217 ± 0.00024
Derived Parameters			
e	Orbital Eccentricity	0.084 +0.032/-0.023	0.066 ± 0.022
ω	Argument of Periastron (°)	41 +23/-34	132 ± 21
Physical Parameters		*Derived*	
M_P	Planet Mass ($M_{♃}$)	$0.613^{+0.027}_{-0.026}$	0.73 ± 0.04
R_P	Planet Radius ($R_{♃}$)	$1.000^{+0.071}_{-0.06}$	1.19 ± 0.02
ρ	Planet Density (gcm^{-3})	$0.76^{+0.17}_{-0.14}$	0.053 ± 0.04
T_{eq}	Equilibrium Temp(K)	1076^{+31}_{-30}	1171 ± 10
M_*	Stellar Mass ($M_\odot$)	$0.864^{+0.041}_{-0.039}$	0.94 ± 0.02
R_*	Stellar Radius ($R_\odot$)	$0.748^{+0.045}_{-0.042}$	0.86 ± 0.01
L_*	Stellar Luminosity ($L_\odot$)	$0.374^{+0.050}_{-0.043}$	-

Table notes: This table outlines the results as presented in two research papers on the K2-29 system, in order to compare our obtained results in a similar fashion to the process automated within HOPS, converting units and uncertainty values for consistency.

[a] All uncertainties provided within (ibid.) are only the statistical ones excluding consideration of the unknown errors on the models.

[b] Stellar parameters are derived from the combined analysis of the data and not from the spectral analysis, with assumed: $1R\odot = 695,508km$, $1M\odot = 1.988\,42\times10^{30}kg$, $1R_{♃} = 71,492km$, $1M_{♃} = 1.898\,52\times10^{27}kg$, $1AU = 149,597,870.7km$.

These quantities provide us with preliminary insight into the system we plan to observe, where, given the similarity of results across numerous observations, reinforces confidence in these quantities as representative of the system. Within the Exoclock II report [7] K2-29b is one of a select number of observations noted to not fall within the primary three light curve quality checks, that is, we see its fitted R_P/R_* curve extends beyond 3σ from literary examples as seen in Table 2. This difference is often induced by the presence of a physical or projected companion, or planets with grazing transits. As such we may anticipate that our model may deviate from expected values slightly given the time between the previous and this observation.

Despite an expectation for some R_P/R_* difference here, many of the results remained within close proximity to prior data, finding $R_P = 1.17R_{♃}$ in the red filter, and $R_P = 1.23R_{♃}$ in the blue. As such, some statistical diagnostic tests are performed on the results at the end of Table 3.

Due to the nature of imaging with a single camera and two filters, each iteration was set to swap the filter and exposure time to alternate between red and blue. Because of this, the $30s$ red exposures had a large gap of $120s$ (blue filter exposure duration), between each capture for that broadband filter, meaning the model had limited data with a comparatively large separation between points to construct from over the duration of the transit. With that, residuals recorded for these observation filters could have been improved through use of multicolour photometry as this increase in information would strengthen the model more than the use of these individual colour filters, so in later observations where we split the data after collecting in multiple wavelengths. We anticipate an improvement from the 5.087‰ standard deviation for red and 6.95‰ for blue, but despite this, the radii ratios measured here fall within the acceptable quality rating, less than one standard deviation from their expected value.

Table 3. Recorded Results for Transit of K2-29b in Two Filters.

Parameter	Description	Filter: R	Filter: B
Orbital Parameters - HOPS			
P_{orb}	Orbital period	3.25883406	3.25883406
T_{mid}	Transit Mid-time	$2459984.3476^{+0.0011}_{-0.0011}$	$2459984.3473^{+0.0014}_{-0.0015}$
R_P/R_*	radius ratio	$0.1404^{+0.0040}_{-0.0042}$	$0.1468^{+0.0082}_{-0.0088}$
			(*expected:* .1419 $\pm$ 0.0006)
i_p	orbital inclination (°)	86.66	86.66
a/R_*	scaled SMA	10.51	10.51
e	Orbital Eccentricity	0.066	0.066
ω	Argument of Periastron	132.0	132.0
$O-C$	Observed-Calculated(mins)	1.35 ± 1.41	0.5 ± 2.16
Derived Parameters			
t_{dur}	transit duration (days)	0.0910	0.0927
τ_{12}	Recorded Ingress(days)	0.0163	0.0179
τ_{34}	Recorded Egress(days)	0.0179	0.0179
δ	transit depth (%)	2.1781	2.5029
a	SMA	0.0420	0.0420
R_P	Planetary Radius ($R_{\odot}$)	1.1747	1.2282
Diagnostic Results			
STD	Residuals Standard Dev (‰)	5.087	6.95
		expected (3.299‰)	expected (1.905‰)
	Transit SNR	17.64	14.55
	Radius Ratio Drift	_0.37 σ	_0.68 σ
	Autocorrelation	0.313	0.232
	Shapiro test	0.01	0.014

Table notes: Presented here are results of our observations with statistical errors displayed where relevant to the fitting routine performed within HOPS, no additional error due to camera gain denoted above.

[a] Derived parameters displaying no calculated error, see Section 4.4.

[b] For unit conversions see Table 2 Notes.

[c] Exposure time for red frames = 30s, for blue frames = 90s.

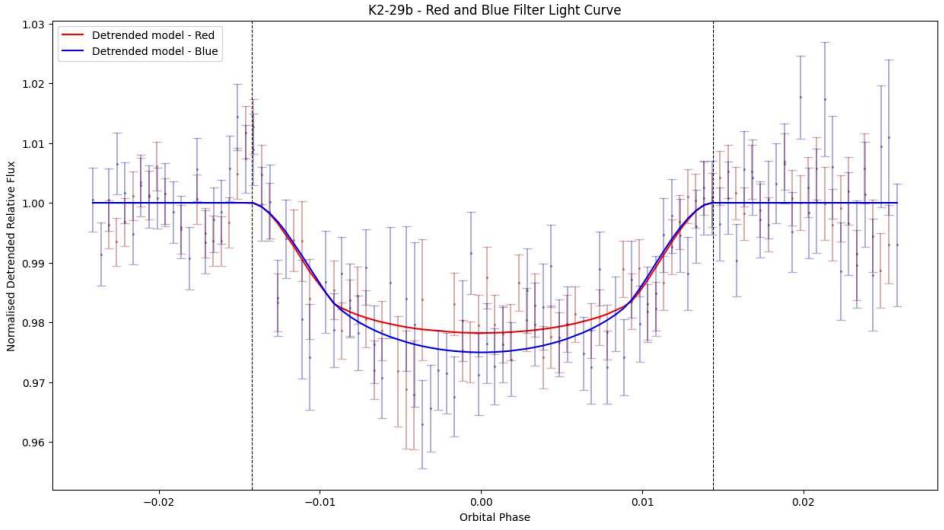

Figure 3. Plot of red and blue filter data points and their respective scaled error bars through- out the observation time series with Airmass De-trended Models for each filter, overlaid on normalised relative flux measurement.

4.3.2 WASP-36b

To assess the viability of defining suitable prediction of binary systems through transit measurement features, the system of WASP-36b has been selected due to seemingly anomalous data evident across different studies with research into this stellar companion in [20, 21].

This system, with a metal-poor G-dwarf star, exhibits unique features which enhance concepts, such as planet-metallicity correlations of hot Jupiter formation and atmospheric properties with modelling across most wavebands presenting concurrent values within 1σ [22, 23]. Recent studies recording reduced uncertainties, refining, and updating the prior measurements highlighted unexpected variation across four passbands and 17 high precision light curves. Running MCMC simulations to directly compare photometric parameters at each passband, where between the g' and z' bands, a large variation with significance greater than 5σ measured planetary radius ratio as increasing drastically in the blue wavelength bands.

Table 4. Research Paper results for WASP-36b.

Parameter	Detail	Smith et al. 2012	Maciejewski et al. 2016
Orbital Parameters			
P_{orb}	Orbital period (days)	$1.5373653 \pm 2.6 \times 10^{-6}$	1.5373639 ± 0.0000014
T_{dur}	transit duration (days)	0.07566 ± 0.00042	–
$\tau_{12} = \tau_{34}$	ingress/egress duration (days)	0.01540 ± 0.00054	–
a/R_*	scaled semimajor axis	5.977 ± 0.082	$5.91^{+0.11}_{-0.10}$
R_P/R_*	radius ratio	0.1384 ± 0.00072	$0.1391^{+0.0011}_{-0.0012}$
δ	transit depth (%)	–	–
b	impact parameter	0.665 ± 0.013	$0.657^{+0.029}_{-0.033}$
i_p	orbital inclination (°)	83.61 ± 0.21	$83.62^{+0.30}_{-0.26}$
a	Semi Major Axis	0.02643 ± 0.00026	0.02641 ± 0.00026
Derived Parameters			
e	Orbital Eccentricity	0	–
ω	Argument of Periastron (°)	Anderson et al. 2011	–
Physical Parameters		*Derived*	
M_P	Planet Mass ($M_{♃}$)	2.303 ± 0.068	2.295 ± 0.058
R_P	Planet Radius ($R_{♃}$)	1.281 ± 0.068	$1.330^{+0.030}_{-0.029}$
ρ	Planet Density (gcm^{-3})	1.096 ± 0.067	$0.976^{+0.070}_{-0.068}$
T_{eq}	Equilibrium Temp(K)	1724 ± 43	–
M_*	Stellar Mass ($M_\odot$)	1.040 ± 0.031	Smith et al. 2012
R_*	Stellar Radius ($R_\odot$)	0.951 ± 0.018	$0.960^{+0.020}_{-0.019}$
L_*	Stellar Luminosity ($L_\odot$)	–	–

Table notes:

[a] Some values presented in (ibid.) are predicted at fixed epoch and period.

[b] For unit conversions see Table 2 Notes.

Evaluated in [24] this measure is beyond considering as residual Rayleigh scattering, or chemical composition of the planet's atmosphere alone [25]. It is speculated that the observed transmission photometry may be caused by the presence of an absorber, which, given a large R_P/R_* drift, could be justified by a stellar companion present in this system.

Results collected from our multicolour observations, presented in Table 5, shows good concurrence with prior research, except for one particular outlier in $R_P/R_* = 0.1661$ +0.0098/-0.0102, this value being 3.01σ from the expected value. Despite such a significant discrepancy following fitting and MCMC routines, this aligns with more recently presented spectrum results in [24] with blue waveband deviation. In an attempt to reduce this difference, instead of fitting to an airmass detrending model, the application of a quadratic detrending produced an R_P/R_* drift of 2.11σ, which is closer to an acceptable range, although still beyond what we would anticipate for a successful model. This result can be observed also in predicted R_P values, where red, greed, and blue debayered bands gave 1.25, 1.32, and $1.57R_{♃}$ respectively, where we see this significant radius increase. In this updated case, we observe very few outliers in the data, with few systematics also, as seen by the Shapiro test = 0.008 and AutoCorrelation = 0.195. This result of a substantial deviation greater than "2σ, coupled with previous studies identifying the light curve shape to be beyond the extent of Rayleigh scattering or limb darkening effects, suggests a second star may be present, however further repeated observations would be required to establish a relationship between this observation and patterns within the same band in other binary systems to evaluate this over time.

Table 5. Recorded WASP-36b Transit in Three Debayered Colour Channels.

Parameter	Filter: R	Filter: G/v	Filter: B
Orbital Parameters - HOPS			
P_{orb} (days)	1.537365595	1.537365595	1.537365595
T_{mid} (days)	$2460037.4211^{+0.0015}_{-0.0015}$	$2460037.4203^{+0.0015}_{-0.0015}$	$2460037.4234^{+0.0020}_{-0.0021}$
R_P/R_*	$0.1352^{+0.0064}_{-0.0067}$	$0.1426\ ^{-0.0063}_{+0.0057}$ (*expected:* .0.1368 $\pm$ 0.0006)	$0.1700\ ^{+0.0012}_{-0.011}$
i_p (°)	83.15	83.15	83.15
a/R_*	5.58	5.58	5.58
e	0.0	0.0	0.0
ω (°)	0.0	0.0	0.0
$O-C$	-2.94 ± 2.3	-3.08 ± 2.3	1.38 ± 3.02
Derived Parameters			
T_{dur} (days)	0.07410	0.07556	0.0785
τ_{12} (days)	0.0145	0.02615	0.0203
τ_{34} (days)	0.0145	0.0203	0.0203
δ	1.8817	2.1115	2.8827
a	5.85	5.85	5.85
R_P ($R_{\odot}$)	1.2508	1.3193	1.5728
Diagnostic Results			
STD	7.295‰ expected (2.87‰)	6.983‰ expected (2.87‰)	13.793‰ expected (3.299‰)
SNR	10.16	11.07	7.38
R_P/R_* Drift	$-0.24\ \sigma$	$0.89\ \sigma$	2.11σ
Autocorrelation	0.209	0.272	0.195
Shapiro Test	0.008	0.009	0.008

Table notes: Presented here are results of our observations with statistical errors displayed where relevant to the fitting routine performed within HOPS, no additional error due to camera gain denoted above.

[a] Derived parameters display no calculated error, see Section 4.4.

[b] For unit conversions see Table 2 Notes.

[c] Exposure time for all frames = 120s.

4.4 Error Calculations

The majority of error calculations within this project are performed through HOPS, where the processing of database and statistical errors provide informative descriptions of the final result, as presented within Tables 3, 5. Error bars in plotted figures such as Figure 3, or 4 are determined here initially by $\sqrt{F + 2 * sky}$. This value is scaled based on the RMS of the residuals of the best fit model plotted in each graph for its respective filter, ensuring uncertainties maintain the correct scale factor post-processing. In general, we observe larger uncertainty in the blue filter results due to Rayleigh scattering, where the upper atmosphere of observed Gas giants possesses increased interference with the shorter wavelengths of light. The derived parameters present no stated uncertainty due to their calculation being directly sourced by available collected data within HOPS's and its partial analysis report. HOPS does not explicitly state all quantities or uncertainties used for calculation, such as R_* or a, these being approximated from past research values where necessary, with the information accessible from the software's processing data. In each of these cases, if absolute uncertainty was provided, each could be calculated by addition of their absolute uncertainties for T_dur, $\tau_1 2$ $\tau_3 4$, where each of these is calculated by subtraction from the best fit model curve, by calculation of the uncertainty's maximum and minimum bounds for values where some range is present, or for multiplication or division terms by calculation of their respective percentage uncertainties, with this being demonstrated above to convert units for consistency where uncertainty values have been available.

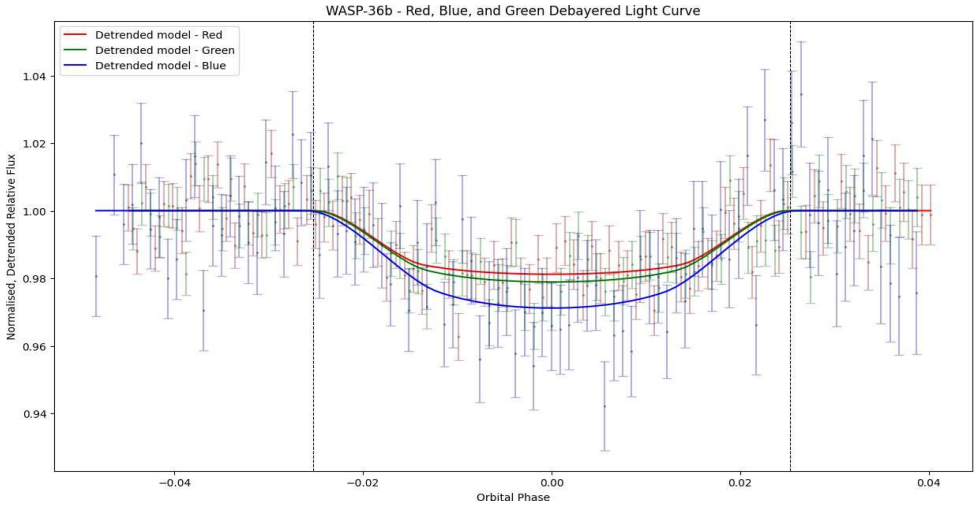

Figure 4. Plot of red, blue and green debayered data points and their respective error bars for WASP-36b, with airmass detrended models for each filter coloured overlaid on the same normalised relative flux measurement.

5. Conclusions

Results presented in this study offer a comprehensive investigation into the viability of multicolour photometry and its benefit to performing accurate exoplanet transit measurement, yielding results consistent with past observations while reducing uncertainty in the ephemerides and parameters which describe such systems. Demonstrating this through application of a debayering routine to obtain consistent results from clear filter observations ensured the application of such a technique maintained strong results, providing further insight into the three-component primary colour channels which collectively portray the system, without the need to cycle filters or operate an array of telescopes. Selected targets of the confirmed exoplanet orbiting a binary star system K2-29b, the less complex TrES-3b and HAT-P-54b have each been well defined in prior surveys to provide a controlled comparison of the pre-processing on more predictable systems. With this knowledge, for the inspection of WASP-36b, a system with a proposed binary star, we anticipated some deviation which was observed in the debayered blue dataset where R_P/R_* = 0.116 +0.0098/-0.0102. Initial MCMC fitting passes using a standard airmass detrending model procured this quantity with drift of +3.01σ which is large for such observations, and particularly in comparison to the red and green debayered drift of -0.24σ and 0.89σ respectively. Applying a more complex quadratic detrending model offered a slight decrease to 0.16 +0.011/-0.012, with drift = 2.11σ, but with this persisting large deviation, we can infer the presence of an absorber in the system, which may be a stellar companion. To substantiate any claim to further characterise an additional body would require additional transit observations to identify flux phases across transit observations which may correlate to a binary orbit pattern, where these could be compared to known systems such as K2-29b. If such a relationship appears, it would enable repeat observation of exoplanetary transit with multicolour photometry to predict the likelihood of multiple star systems, similarly to TTV suggesting additional planetary bodies.

Acknowledgements

To begin on a professional level, I shall first thank my supervisors, Professor Daniel Thomas, Dr Hooshyar Assadullahi, and Steve Futcher, who were instrumental in facilitating this project in collaboration with Clanfield Observatory, providing support throughout its duration and guiding both objectives and milestones through periodic meetings and discussion of completed work.

Particular thanks go to Steve Futcher for imparting his expertise in the field of astronomy and exoplanet observations, educating me on the nuance of observations and the operational procedure to successfully capture an exoplanet's transit; also offering so much of his time in transportation and the full duration of observation time which often stretched into the early hours of the morning. An extension of this thanks goes to the Hampshire Astronomical Group for their collective experience in the use and upkeep of research-grade equipment, along with some late-night problem solving, results discussion, and finally for being so welcoming to students requesting access to equipment on the few clear nights the months presented. Thank you to Dr Hooshar Assadullahi for your persisting optimism and passion for physics, offering so much of your time to support BSc Physics and Astrophysics projects. And finally, I would like to thank Professor Daniel Thomas for his guidance in meeting the requirements for the university within the project, and highlighting the importance of each component of this research for constructing a thorough scientific narrative in a field of Physics I was far less familiar with prior to this project.

On a personal level, I would like to thank my peers, who while completing their own research have offered suggestion and discussion which has led to my deeper understanding of this topic. Notably Sanel Kartal who, in conducting similar research at a higher level, investigating atmospheric effects, has shared in some of the challenges along the development of this project, providing generously her knowledge of concepts and research of the vast topics within this aspect of observational astronomy. Last but certainly not least, Isobel Smith-Maryan for her faith in my ability to complete this project and for consoling me in moments when my optimism faltered, continuing to be the rational voice at every step.
As mentioned briefly above, a particular challenge for observations at this time of year is finding suitable conditions under which to gather data, and as such I am grateful that Dominique Daniel kindly offered to share his files of repeated observation data for TrES-3b using red, blue filters and clear filters across multiple observation sessions. Having observation data to test and validate the computational work completed within this project was instrumental in the efficient processing once conditions became more reliable.

Notes

[N1] The photometry measure of light or flux through multiple colour filters, from an exoplanet's host star as the planet orbits, appearing to transit across the star's surface.
[N2] A class of exoplanet with short orbital periods of $P < 10$ days and large planetary masses $M_P > 0.1 M_{♃}$ (Jupiter masses). This classification of gas giants makes up over 32% of confirmed exoplanets [26].
[N3] The vertical distance by which the planet's centre point is offset from the stellar centre point from the observer's perspective.
[N4] Feature of a star described by the radiative transfer physics of stellar atmospheres, see Appendix F for additional description.
[N5] In a monochrome camera, the read noise across the sensor is the standard deviation of expected photons detected against recorded photons in each pixel square. To perform binning, we sum across the binning size, e.g. 2*x*2, and take those squares, e.g. 4, and take these to be the count across that entire region, e.g. 4 squares, producing one square of four times the size.

References

[1] Dragomir, Diana, Johanna Teske, et al. (2019), TESS Delivers its first earth-sized planet and a warm Sub-Neptune, The Astrophysical Journal Letters 875.2, p. L7.
[2] Wang, Gavin and Karen Collins (2021), Analyzing FFIs to Identify False Positives within TESS Candidates, Posters from the TESS Science Conference II (TSC2), p. 19.
[3] Tinetti, Giovanna et al. (2021), Ariel: Enabling planetary science across light-years, arXiv preprint arXiv:2104.04824.
[4] Miles, Brittany E et al. (2023), The JWST Early-release Science Program for Direct Observations of Exoplanetary Systems II: A 1 to 20 μm Spectrum of the Planetary-mass Companion VHS 1256–1257 b, The Astrophysical Journal Letters 946.1, p. L6.
[5] Espinoza, Néstor and Andrés Jordán (2015), Limb darkening and exoplanets: testing stellar model atmospheres and identifying biases in transit parameters, Monthly Notices of the Royal Astronomical Society 450.2, pp. 1879–1899.
[6] Kokori, A, A Tsiaras, B Edwards, A Jones, et al. (2023), ExoClock Project. III. 450 New Exoplanet Ephemerides from Ground and Space Observations, The Astrophysical Journal Supplement Series 265.1, p. 4.
[7] Kokori, A, A Tsiaras, B Edwards, M Rocchetto, et al. (2022), ExoClock Project. II. A Large-scale Integrated Study with 180 Updated Exoplanet Ephemerides, The Astrophysical Journal Supplement Series 258.2, p. 40.
[8] Kokori, Anastasia et al. (2022), ExoClock project: an open platform for monitoring the ephemerides of Ariel targets with contributions from the public, Experimental Astronomy 53.2, pp. 547–588.
[9] Murgas, F et al. (2014), The GTC exoplanet transit spectroscopy survey-I. OSIRIS transmission spectroscopy of the short period planet WASP-43b, In: Astronomy & Astrophysics 563, A41.
[10] Haswell, Carole A. (2010) "Chapter" in: Transiting Exoplanets. Cambridge Univ. Press.
[11] Wilson, Paul Anthony (2021), The exoplanet transit method PaulAnthonyWilson.com | Observational Astronomer. url: https://www.paulanthonywilson.com/exoplanets/exoplanet-detection-techniques/the-exoplanet-transit-method/.
[12] Essick, Reed and Nevin N Weinberg (2015), Orbital decay of hot Jupiters due to nonlinear tidal dissipation within solar-type hosts, The Astrophysical Journal 816.1, p. 18.
[13] Mandel, Kaisey and Eric Agol (2002), Analytic light curves for planetary transit searches, The Astrophysical Journal 580.2, p. L171.
[14] Seager, Sara and Gabriela Mallen-Ornelas (2003), A unique solution of planet and star parameters from an extrasolar planet transit light curve, The Astrophysical Journal 585.2, p. 1038.
[15] Yee, Samuel W, Joshua N Winn, and Joel D Hartman (2021), How Complete Are Surveys for Nearby Transiting Hot Jupiters? The Astronomical Journal 162.6, p. 240.
[16] Tsiaras, Angelos (2019), HOPS: the photometric software of the HOlomon Astronomical Station, Epsc-dps joint meeting 2019. Vol. 2019, EPSC–DPS2019.
[17] Kokori, Anastasia (2021), Exoworlds Spies|Observing an exoplanet transit, https://www.exoworldsspies.com/en/observers/.
[18] Kim, Dae-Won et al. (2009), Detrending time series for astronomical variability surveys, Monthly Notices of the Royal Astronomical Society 397.1, pp. 558–568.
[19] Santerne, A et al. (2016), K2-29 b/WASP-152 b: An aligned and inflated hot Jupiter in a young visual binary, The Astrophysical Journal 824.1, p. 55.
[20] Ngo, Henry et al. (2016), FRIENDS OF HOT JUPITERS. IV. STELLAR COMPANIONS BEYOND 50 au MIGHT FACILITATE GIANT PLANET FORMATION, BUT MOST ARE UNLIKELY TO CAUSE KOZAI–LIDOV MIGRATION, The Astrophysical Journal 827.1, p. 8.
[21] Evans, DF et al. (2016), High-resolution Imaging of Transiting Extrasolar Planetary systems (HITEP)-I. Lucky imaging observations of 101 systems in the southern hemisphere, Astronomy & Astrophysics 589, A58.
[22] Maciejewski, G et al. (2016), New transit observations for HAT-P-30 b, HAT-P-37 b, TrES-5 b, WASP-28 b, WASP-36 b, and WASP-39 b". In: arXiv preprint arXiv:1603.03268.
[23] Smith, AMS et al. (2012), WASP-36b: A new transiting planet around a metal-poor G-dwarf, and an investigation into analyses based on a single transit light curve, The Astronomical Journal 143.4, p. 81.
[24] Mancini, Luigi et al. (2016), An optical transmission spectrum of the giant planet WASP-36 b, Monthly Notices of the Royal Astronomical Society 459.2, pp. 1393–1402.
[25] Dragomir, Diana, Björn Benneke, et al. (Nov. 2015), RAYLEIGH SCATTERING IN THE ATMOSPHERE OF THE WARM EXO-NEPTUNE GJ 3470B, The Astrophysical Journal 814.2, p. 102. doi:https://dx.doi.org/10.1088/0004-637X/814/2/102.
[26] NASA (2023), Exoplanet Exploration: Planets Beyond Our Solar Syste. url: https://exoplanets.nasa.gov/.

Acronyms

ARIEL Atmospheric Remote-sensing Infrared Exoplanet Large-survey.

FOV Field of View.

HOPS HOlomons Photometric

Software. JWST James Webb Space

Telescope.

LDC Limb Darkening

Coefficient. MCMC Markov chain

Monte Carlo.

RMS Root Mean
Square. RV Radial
Velocity.

SNR Signal to Noise Ratio.

TESS Transiting Exoplanet Survey
Satellite. TTV Transit Timing Variation.

Appendix A
K2-29b - Additional Results and Plots

A.1 K2-29b, Filter Plots

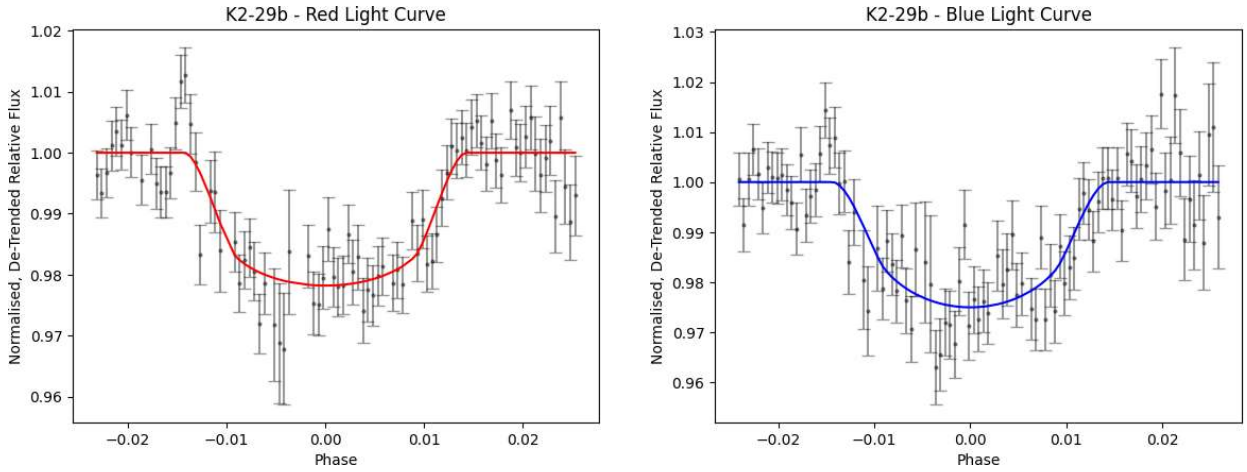

Figure 5. Plot for the Detrended model of K2-29b Red Filter images (*Left*); Plot for the Detrended model of K2-29b Red Filter images (*Right*).

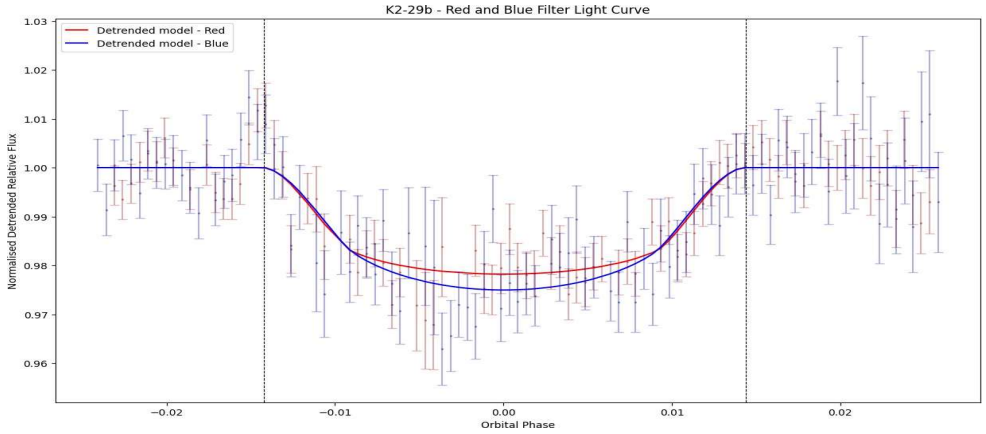

Figure 6. Plot of red and blue filter collected data relative in the Airmass De-trended Model.

A.2 K2-29b - ExoClock / HOPS Figures

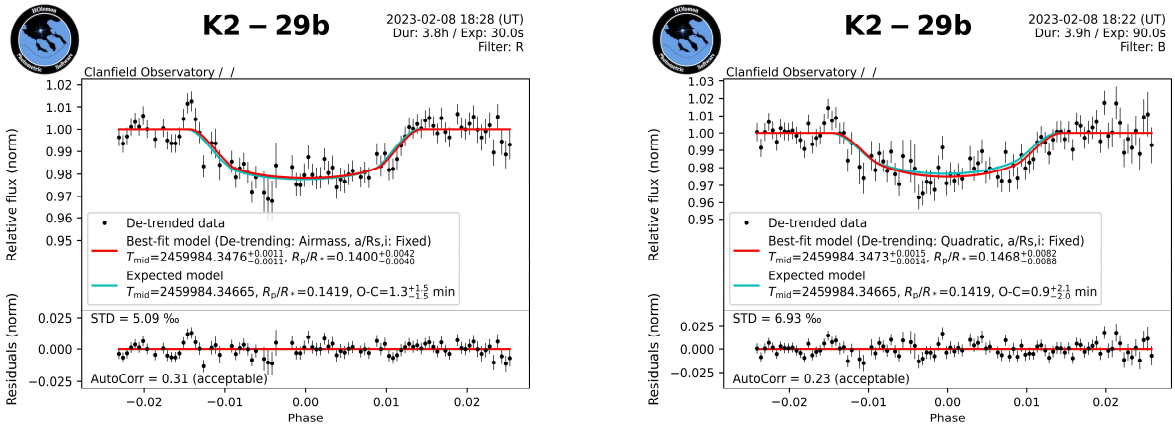

Appendix B
TrES-3b - Results with Additional Data and Plots

B.1 TrES-3b Results

To ensure the correct procedure for debayering an image and how it can expand upon the data available from a full colour image, we compare the results collected by Dominique Daniel. The two observations considered within this study are observations of the same exoplanet target, TrES-3b, in both individual red and blue filters, Table 7 as well as using a full colour clear filter.

Table 7. TrES-3b Results as presented by Daniel, D.

Parameter	Detail	Filter: R	Filter: B
Orbital Parameters			
P_{orb}	Orbital period (days)	1.30618639	1.30618639
$T0$	transit epoch (BJD0)	$2459840.388^{+0.003}_{-0.002}$	$2459840.3901^{+0.0028}_{-0.0019}$
a/R_*	scaled semimajor axis	6.0	6.0
R_P/R_*	radius ratio 0.1373	$0.169^{+0.021}_{-0.018}$	0.135^{+}
i_p	orbital inclination (°)	82.0	82.0
Derived Parameters			
ω	Argument of Periastron (°)	0.0	0.0
a	Semi Major Axis	6.0	6.0
e	O-C	$-6.2^{+0.003}_{-0.002}$	$-3.2^{+4.0}_{-2.7}$

B.2 TrES-3b Plots

B.2.1 TrES-3b - Filter Plots

Presented in this section are the plots displaying data collected using separate filters to observe the transit of TrES-3b.

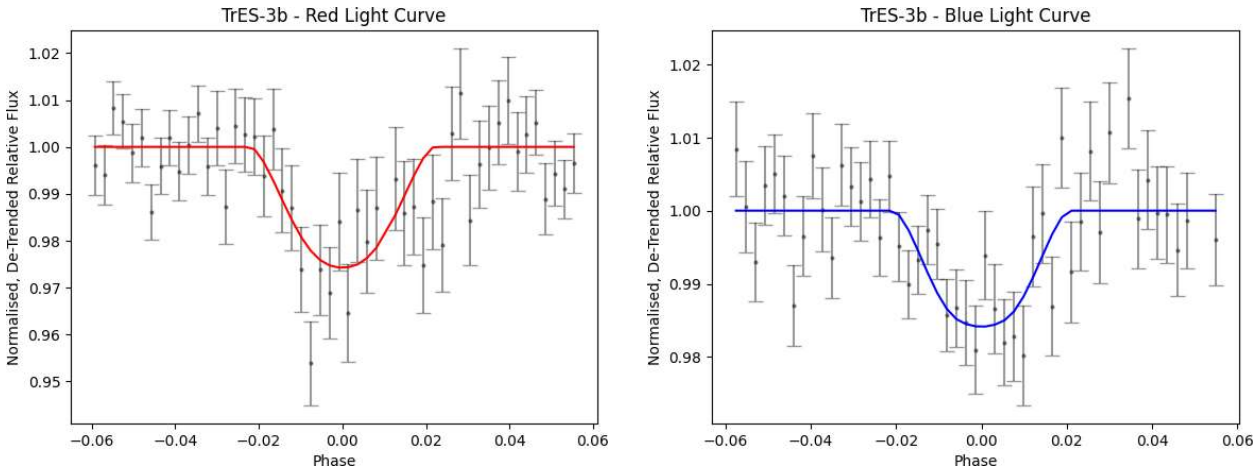

Figure 7. Plot for the Detrended model of K2-29b Red Filter images (*Left*); Plot for the Detrended model of K2-29b Red Filter images (*Right*).

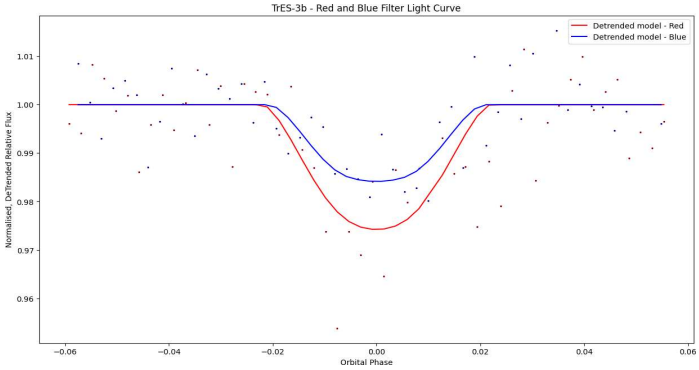

Figure 8. Plot of red and blue filter collected data relative in the Airmass De-trended Model.

B.3 TrES-3b - ExoClock / HOPS figures

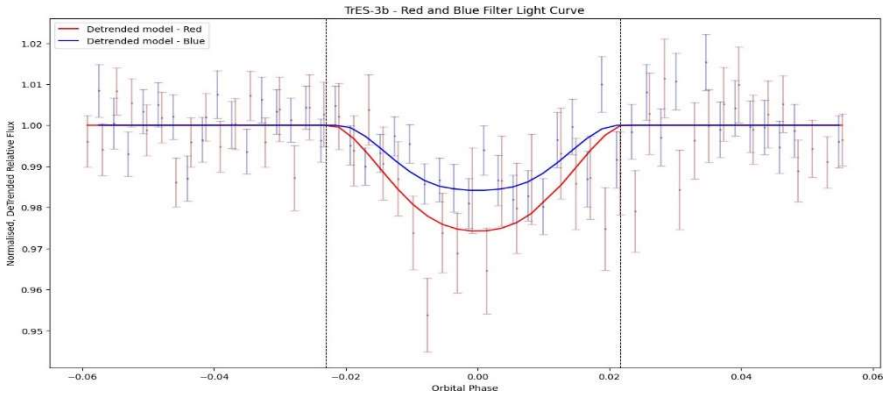

Figure 9. Plot of red and blue filter collected data relative with error bars for datapoints in the Airmass De-trended Model.

Appendix C
WASP-36b, Additional Results and Plots

C.1 ExoClock / HOPS figures

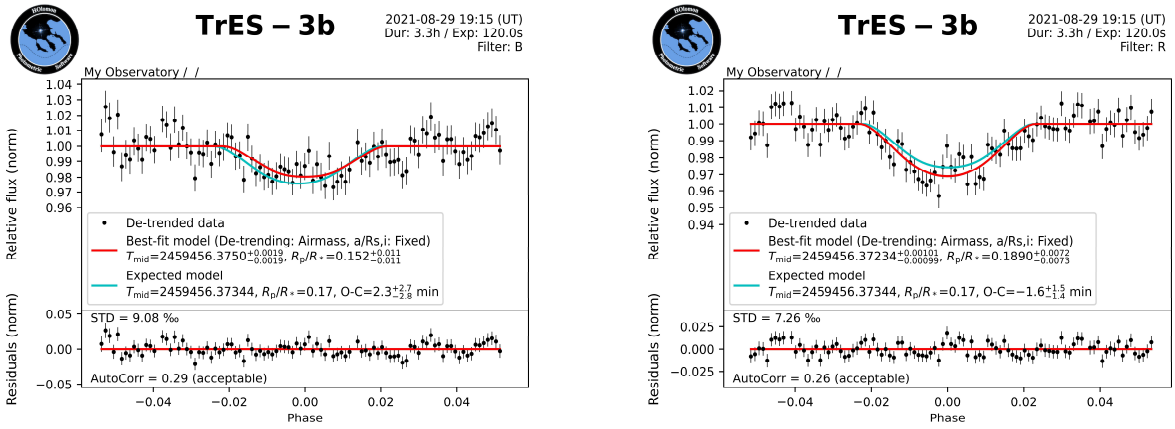

Figure 10. (*Left*) Exoclock plot for the detrended model of TrES-3b Red debayered image; (*Right*) Exoclock plot for the detrended model of WASP-36b Green debayered image.

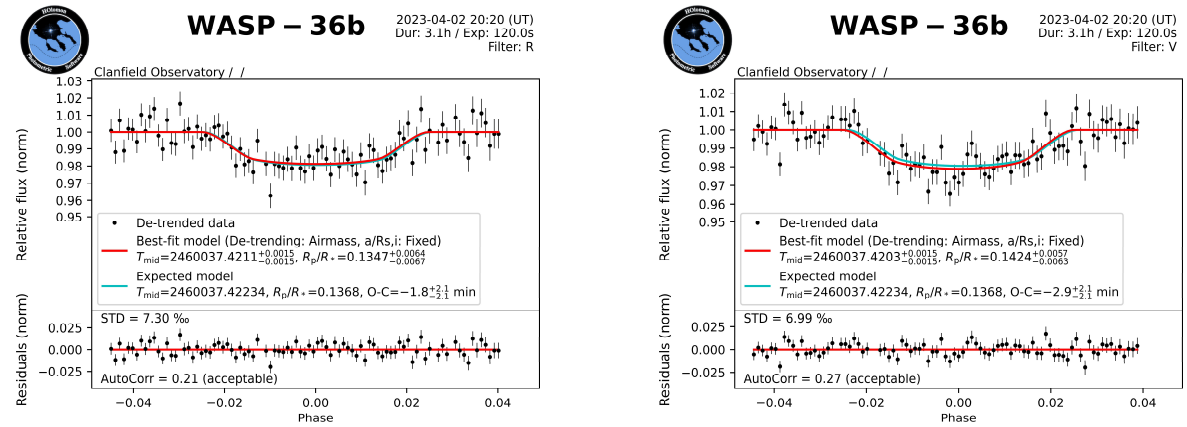

Figure 11. (*Left*) Exoclock plot for the detrended model of WASP-36b Red debayered image; (*Right*) Exoclock plot for the detrended model of WASP-36b Green debayered image.

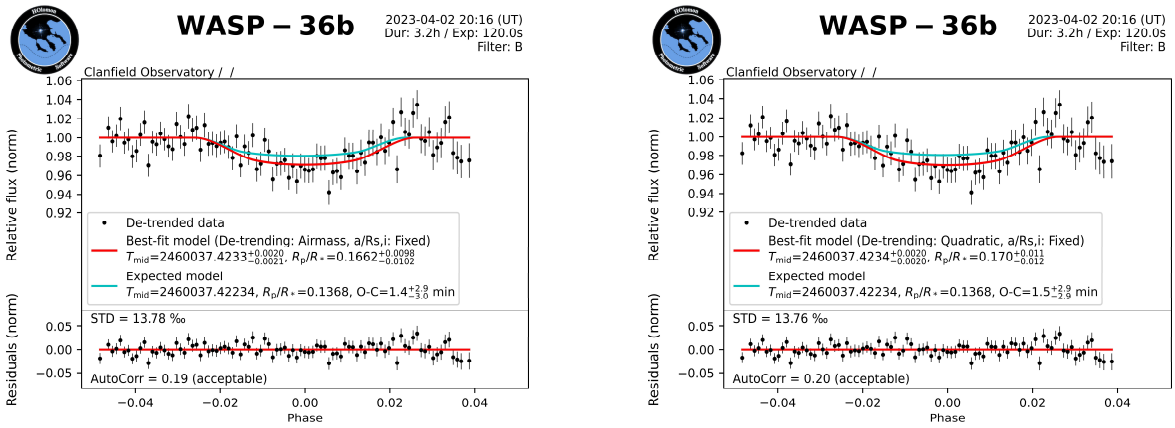

Figure 12. (*Left*) Exoclock plot for the Airmass detrended model of WASP-36b Blue debayered image; (*Right*) Exoclock plot for the Quadratic detrended model of WASP-36b Blue debayered image.

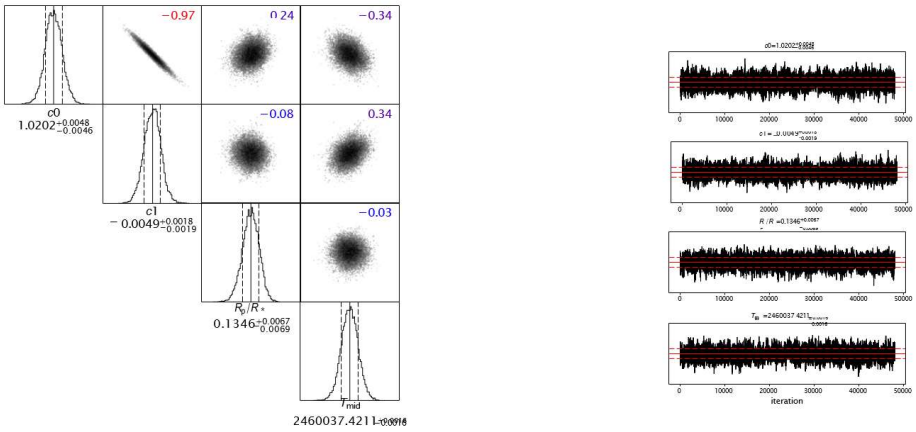

Figure 13. (*Left*) Corner plots for the two limb darkening coefficients used to model WASP-36b Red debayered image, and radius ratio distribution; (*Right*) Traces plot for WASP-36b Red debayered image for each variable considered in the model construction.

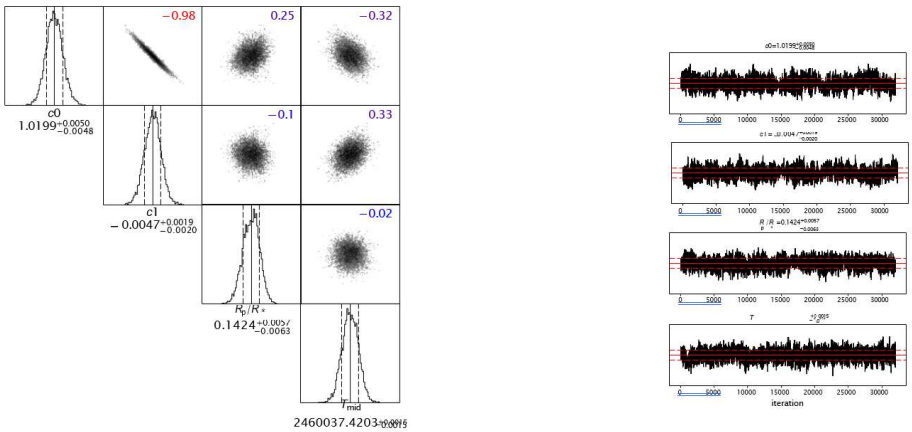

Figure 14. (*Left*) Corner plots for the two limb darkening coefficients used to model WASP- 36b Green debayered image, and radius ratio distribution; (*Right*) Traces plot for WASP-36b Green debayered image for each variable considered in the model construction

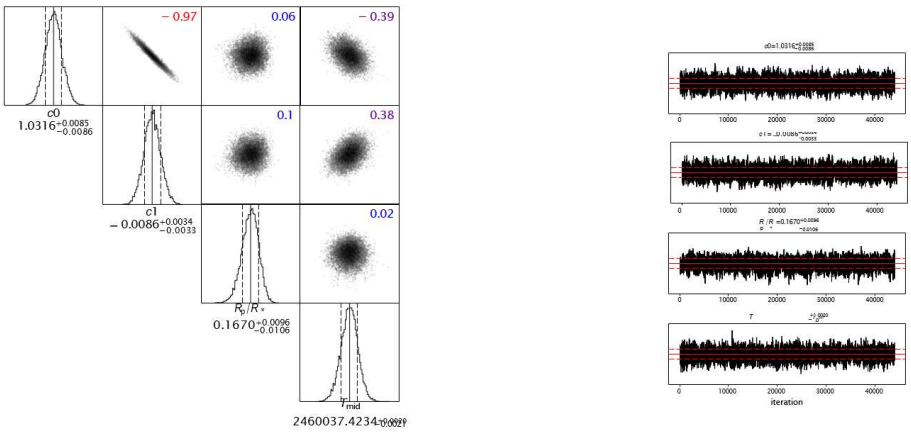

Figure 15. (*Left*) Corner plots for the two limb darkening coefficients used to model WASP-36b Blue debayered image, and radius ratio distribution; (*Right*) Traces plot for WASP-36b Blue debayered image for each variable considered in the model construction.

Appendix D
HAT-P-54b, Results and Plots

Even a partial transit light curve improves the precision of the measured system parameters enormously compared to those derived solely from the WASP photometry and the RVs. Smith et al. 2012

D.1 Exoclock / HOPS Figures

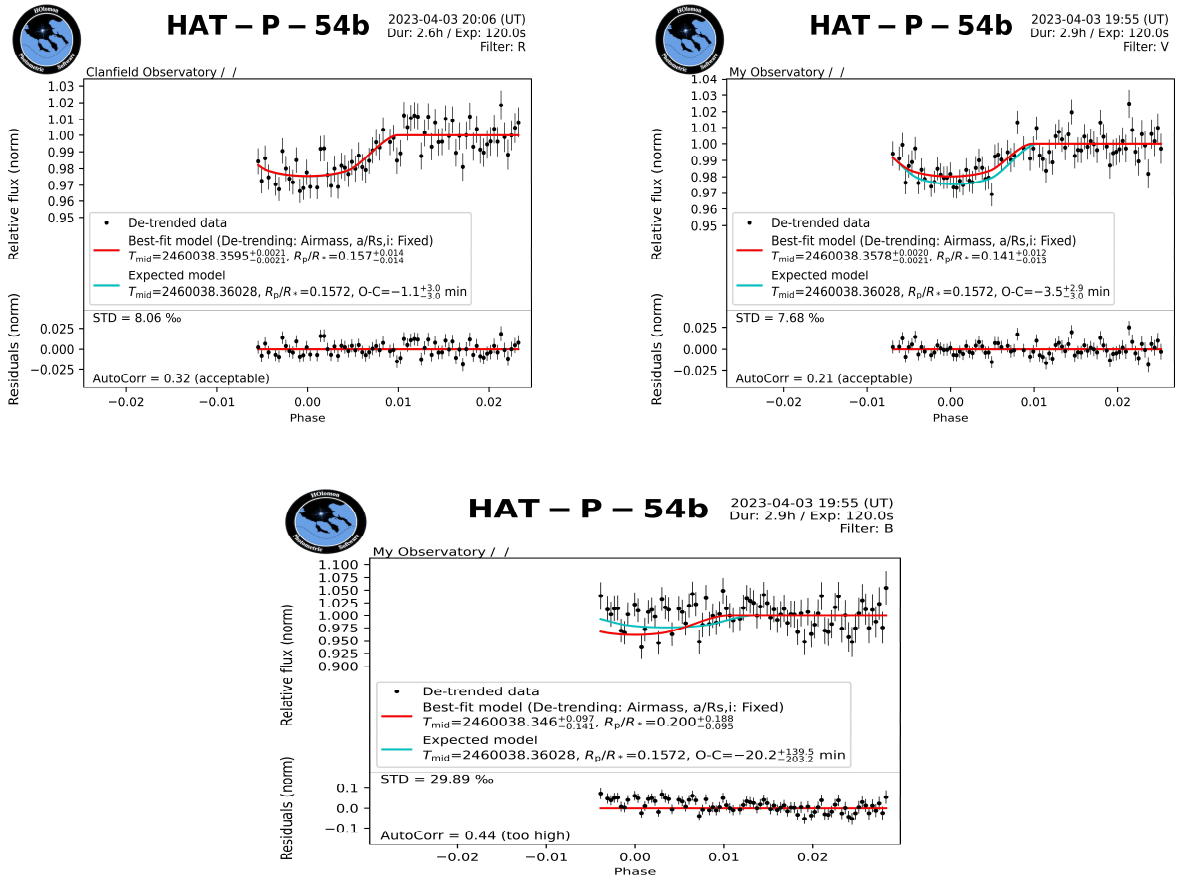

Figure 16. (*Left*) Exoclock plot for the Airmass detrended model of HAT-P-54b Red debayered image; (*Right*) Exoclock plot for the Airmass detrended model of HAT-P-54b Visual debayered image; (*Lower*) Exoclock plot for the Airmass detrended model of HAT-P-54b Blue debayered image;

Appendix E
Theory and Derivations

E.1 The Radius Ratio Derivation

To define the radius ratio which relates the change in apparent flux to the exoplanet and stellar radii is a simple relation given that at the large distance of observation relative to the spherical shape of these objects, we can approximate each body as the area of a sphere.

$$A = \pi r^2 \tag{4}$$

The change in flux therefore is observed to be the fraction of the stellar surface blocked during the transit compared to before the transit, where this is proportional to the surface area of the planet which covers an area of the total stellar surface area.

$$\frac{Area_{Blocked}}{Area_{Total}} = \frac{\pi r_{Blocked}^2}{\pi r_{Total}^2} \tag{5}$$

Finally, we reach the equation seen in Section 2.1, as π terms cancel, giving our equation for the flux observed during transit.

$$\frac{\Delta F}{F} = \left(\frac{R_P}{R_*}\right)^2 \tag{6}$$

E.2 Transit Duration

Simplification of this derivation can be made given some rarely observed yet foundational assumptions to construct a simplistic system from which the duration of transit presented in the above documentation, Section 2.2 is defined. We begin in the $b = 0.0$ case, where the transit passes through the observed centre point of its star. In this case, the transit duration can trivially be defined as a fraction of one orbital period, where given $R_P >> R_*$, the arc length VW crossed for one complete transit approximates to the diameter of the star R_*, Figure 18.

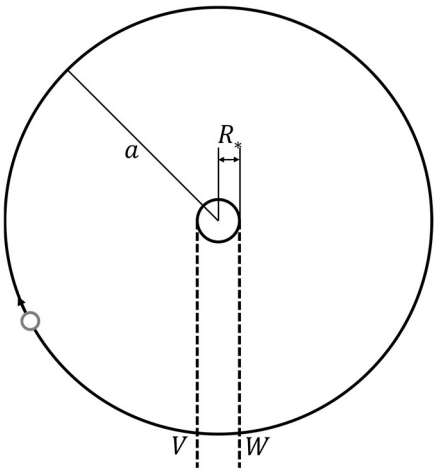

$$T_{dur} = P\frac{ArcLength_{VW}}{Cicumference_{Orbit}} \approx P\frac{2R_*}{2\pi a} \approx \frac{PR_*}{\pi a} \tag{7}$$

Figure 17. Diagram displaying approximation of arc length VW and stellar diameter, $2R_*$ (*Left*) Equation for the fraction of the total orbital period, P, over which the planet passes, equivalent to, $2R_*$, over the entire orbit path where semi-major axis, a. (*Right*).

E.2.1 Semi-Major Axis

Using a generalisation of Kepler's third law, whereby we assume stellar mass to be far greater than planetary mass, as is the case in the majority of observations, we can state that for $M_* >> M_P$, we find the semi-major axis:

$$\frac{a^3}{P^2} = \frac{G(M_* + M_P)}{4\pi^2} \tag{8}$$

$$a = \sqrt[3]{P\frac{G(M_* + M_P)}{4\pi^2}} \approx \left(GM_*\left(\frac{P}{2\pi}\right)^2\right)^{1/3} \tag{9}$$

E.2.2 Pythagorian Transit Distance

Constructing the maximum distance across which the planet transits where *b* is non-zero, following Equation 2.2, we can define the new length *l* of the path. To measure the time elapsed for a circular orbit we can consider Figure 19 for the duration in the generalised circular orbit case, where *α* is the angle in radians between *V* and *W:*

$$T_{dur} = P\frac{\alpha}{2\pi} \tag{10}$$

$$\sin\left(\frac{\alpha}{2}\right) = \frac{l}{a} \tag{11}$$

$$\alpha = 2\sin^{-1}\left(\frac{l}{a}\right) \tag{12}$$

Inserting Equation 12 into Equation 10 we reach the final result as presented within Section 2.2 after *l* is substituted for its definition from Equation 15.

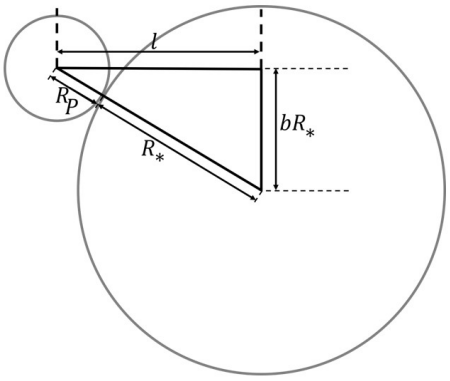

$$a^2 = b^2 + c^2 \tag{13}$$

$$(R_* + R_P)^2 = (bR_*)^2 + (l)^2 \tag{14}$$

$$l = \sqrt{(R_* + R_P)^2 - (bR_*)^2} \tag{15}$$

Figure 18. Diagram from Observer's perspective where planet is at beginning of egress, where we observe initial drop in flux (*Left*); Equation for path length of transiting planet with non- zero impact parameter(*Right*).

$$T_{dur} = \frac{2P}{\pi}\sin^{-1}\left(\frac{l}{a}\right) \tag{16}$$

$$= \frac{P}{\pi}\sin^{-1}\left(\frac{\sqrt{(R_*+R_P)^2-(bR_*)^2}}{a}\right) \tag{17}$$

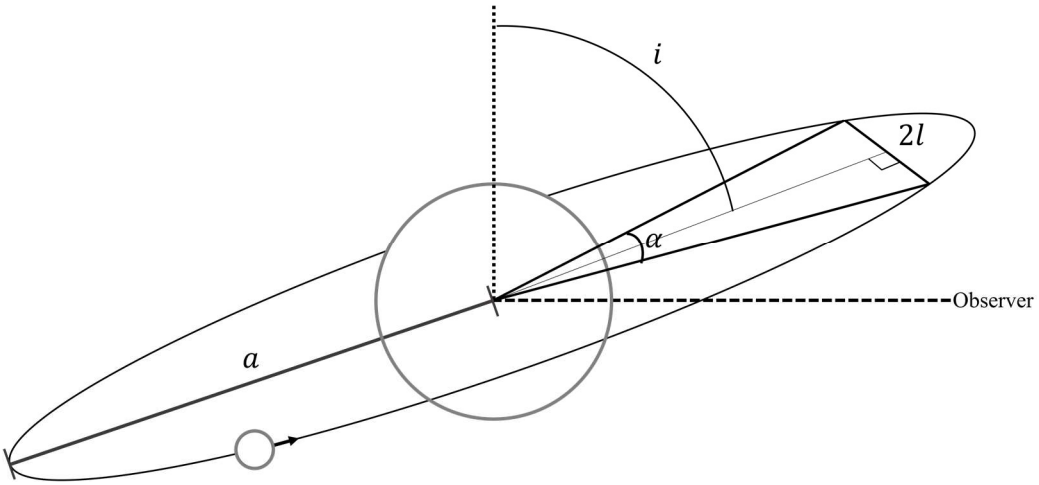

Figure 19. Diagram to illustrate approximations made and terms within T_{dur} equation for non-equatorial orbit.

Appendix F
Photometry and Ground Based Observations

F.1 Limb Darkening

Limb darkening is the decrease in the apparent magnitude of the stellar disk from bright centre to dimmer edges or the progressively darker limbs. The presence of limb darkening can be observed within a light curve as mentioned above where it approaches a parabolic shape across its dipped region, where this effect interferes with measurement. When measuring the flux change, ΔF, this value is observed at the point of transit farthest from the limb of the stellar surface area to assess the maximum change in saturation of the recording. The rarely uniform nature of this effect given the presence of irregularities such as dark sunspots (C. A. Haswell 2010), we apply multiple LDC even for the $b = 0.0$ case. To avoid biases in the data when performing fitting, it is optimal to not define set parameters outside of stellar mass, as in many cases the assumptions and descriptive precision of these models particularly due to a lack of complete knowledge of how stellar intensity evolves and is distributed over time, leads to inaccuracies in the model.

$$\frac{I(\mu)}{I(1)} = 1 - u(1-\mu) \tag{18}$$

$$\frac{I(\mu)}{I(1)} = 1 - u(1-\mu) - v_l \mu \ln \mu \tag{19}$$

$$\frac{I(\mu)}{I(1)} = 1 - u_q(1-\mu) - v_q(1-\mu)^2 \tag{20}$$

Given so many dependencies, great variation is observed between stars, and as such we can define laws based on detailed and continuous close study of our Sun described within (Espinoza and Jordán 2015) in detail. Above are the three most recurring 18 adopting for intensity emitted at an angle $\arccos \mu$ for the linear law, 19 for the logarithmic law, and finally 20 for the quadratic law.

In a general case however, we observe that longer wavelengths, as apparent in red and green filter observations within which the model curve appears more flattened at its base, compared to shorter wavelengths where the transit light curve base appears more rounded in many plots above.

Appendix G
Debayering Images in Python and Calibration Frames

Debayering is the process whereby the colour channels of a picture are split into their respective components as a colour camera sensor for the CCD/CMOS equipment often used in astronomy features a Bayer pattern, where pixels are arranged in a 2x2 grid, often RGGB or GRBG configurations. To take advantage of observation time, instead of using colour filters and only collecting one band of light from a single observation, by utilising the full multicolour sensor, we can perform some pre-processing of the images to withdraw the red, blue, and green channels. This process inherently reduces the resolution detail of an image to maintain the correct size we must interpolate from known to blank pixel spaces where the removed channels were, however by performing binning as well as the noise reduction routines of bias dark and flat frames, the loss here is negligible in comparison to the additional data these provide. We perform this routine on the light frames themselves as well as for the bias, dark, and flats. Bias and dark frames can simply be directly duplicated across as Appendix G.1.3 details, given that both are universal across all channels, where bias provides camera's baseline noise with no exposure (cap covering optics) recorded at the correct cooled temperature during observation; dark frames provide a similar baseline, but at with an exposure time matching the light frames also at observation temperature. The flat frames, however, are taken for constant illumination across the entire field of view to highlight any inherent errors or variations in the optical system where a harsh gradient between pixels may induce incorrect results when imaging, where we captured dusk sky or directed towards a constant light source surface, capturing at 2/3 of the cameras full well depth.

G.1 Python Debayering Psuedocode

Both light and flat frames both contain information describing pixels with desired full colour information, and as such both require the complete debayer process to save this information into the target destination for red, green and blue '.fits' files.

- Define file path locations to access '.fits' files, allowing the program to sort through the list at each step to pick out subsequent images to perform debayer routine on.
- Identify correct Bayer pattern for RGGB, BGGR, GBRG, or GRBG.
- Open '.fits' files in loop, saving Header Data Unit (HDU) and extracted data, building an array for each colour channel without header information
- Set Primary HDU to encapsulate the the data for the '.fits' file.
- Use openCV package for splitting all pixel data information into a tuple of three colour channels.
- Assign each colour to arrays of their respective colours to append after header information in following steps.
- For each colour channel:
    - Set Primary Header Data Unit, applying this list to the iteration's colour Header Data.
    - Introduce all Header Data beyond Primary, including 'Filter' information
    - Add all relevant data from tuple of this iteration to image to complete the '.fits' file with data and classifying header information
    - Save file to relevant 'Split_X' folder and move on to next colour or next step of iteration through files.
- Load image data and Header Data Unit List information from save path to ensure all values represented and stored correctly in '.fits' format.

G.1.1 Python Debayering Code - Light Frames

```
from astropy.io import fits
from astropy.utils.data import download_file
from astropy.visualization import astropy_mpl_style
import numpy as np
import matplotlib.pyplot as plt
import os
from os.path import exists
import cv2

from google.colab import drive
drive.mount('/content/drive', force_remount=True)
from pathlib import Path

# Defining File Path through iteration of generated list
for num in range(1,94,1):
    Root_dirA = '/content/drive/MyDrive/Project/Debayer Code and Files/WASP-36b/Wasp-36b-{:04d}'.format(num)
# Construction of full file path at each number iteration
    Root_dirB = "Col.fit"
    Root_dir_TOT = Root_dirA + Root_dirB

# Define save directory for Red, Green, and Blue images
    Save_dirA_R = '/content/drive/MyDrive/Project/Debayer Code and Files/WASP-36b/Split_R/Wasp-36b-{:04d}'.format(num)
    Save_dirB_R = "R.fit"
    Save_dirA_G = '/content/drive/MyDrive/Project/Debayer Code and Files/WASP-36b/Split_G/Wasp-36b-{:04d}'.format(num)
    Save_dirB_G = "G.fit"
    Save_dirA_B = '/content/drive/MyDrive/Project/Debayer Code and Files/WASP-36b/Split_B/Wasp-36b-{:04d}'.format(num)
    Save_dirB_B = "B.fit"

# Construction of full file path at each number iteration
    Save_dir_TOTR = Save_dirA_R + Save_dirB_R
    Save_dir_TOTG = Save_dirA_G + Save_dirB_G
    Save_dir_TOTB = Save_dirA_B + Save_dirB_B

# Open fits file at root location, set Header Data Unit
    with fits.open(Root_dir_TOT) as hdul:
        fits_data = hdul[0].data;
        hdu = fits.PrimaryHDU()
        hdr = hdul[0].header
# Full Header data as seen at the start of fits document,
# Contains 43 parameters


# Use openCV to split picel info. to tuple of the 3 colours
        fits_data_split = cv2.cvtColor(fits_data,cv2.COLOR_BayerRGGB2RGB)
# For alternative Bayer Pattern:
        #fits_data_split = cv2.cvtColor(fits_data,cv2.COLOR_BayerGRBG2RGB)
        fds_R, fds_G, fds_B = cv2.split(fits_data_split)

        #Create Red Image
        hdu_R = fits.PrimaryHDU(fds_R)
        hdul_R = fits.HDUList([hdu_R])
        hdul_R[0].header = hdr
        hdr_R = hdul_R[0].header
# Add filter information to header section. - now 44 parameters
```

```
        hdr_R['Filter'] = "TR"
# Save file to location with correct formatted number
        hdul_R.writeto(Save_dir_TOTR,overwrite = True)


        #Create Green Image
        hdu_G = fits.PrimaryHDU(fds_G)
        hdul_G = fits.HDUList([hdu_G])
        hdul_G[0].header = hdr
        hdr_G = hdul_G[0].header
# Add filter information to header section. - now 44 parameters
        hdr_G['Filter'] = "TG"
# Save file to location with correct formatted number
        hdul_G.writeto(Save_dir_TOTG,overwrite = True)


        #Create Blue Image
        hdu_B = fits.PrimaryHDU(fds_B)
        hdul_B[0].header = hdr
        hdr_B = hdul_B[0].header
# Add filter information to header section. - now 44 parameters
        hdr_B['Filter'] = "TB"
# Save file to location with correct formatted number
        hdul_B.writeto(Save_dir_TOTB,overwrite = True)
```

Listing 1: Python Debayer Code for Light Frames.

G.1.2 Python Debayering Code - Flat Frames

```
#Loop through Flat frames to split files, saving to to Split_R, Split_G, Split_B folders
for num in range(1,16,1):
     Root_dirA = '/content/drive/MyDrive/Project/Debayer Code and Files/Dominique_Collection/TrES-3b_2022-07-11_ASI2600MC_RGGB_180s/Flats_100pc_FZ_T10_G101_Off50_51ms_2022-06-01_F_1x1__G101_O50_T-9.60_E0.05s_{:04d}'.format(num)
     Root_dirB = ".fits"
     Root_dir_TOT = Root_dirA + Root_dirB

     Save_dirA_R = '/content/drive/MyDrive/Project/Debayer Code and Files/Dominique_Collection/TrES-3b_2022-07-11_ASI2600MC_RGGB_180s/Split_R/Flats_100pc_FZ_T10_G101_Off50_51ms_2022-06-01_F_1x1__G101_O50_T-9.60_E0.05s_{:04d}'.format(num)
     Save_dirB_R = "Flat_R.fit"
     Save_dirA_G = '/content/drive/MyDrive/Project/Debayer Code and Files/Dominique_Collection/TrES-3b_2022-07-11_ASI2600MC_RGGB_180s/Split_G/Flats_100pc_FZ_T10_G101_Off50_51ms_2022-06-01_F_1x1__G101_O50_T-9.60_E0.05s_{:04d}'.format(num)
     Save_dirB_G = "Flat_G.fit"
     Save_dirA_B = '/content/drive/MyDrive/Project/Debayer Code and Files/Dominique_Collection/TrES-3b_2022-07-11_ASI2600MC_RGGB_180s/Split_B/Flats_100pc_FZ_T10_G101_Off50_51ms_2022-06-01_F_1x1__G101_O50_T-9.60_E0.05s_{:04d}'.format(num)
     Save_dirB_B = "Flat_B.fit"

```

```
14      Save_dir_TOTR = Save_dirA_R + Save_dirB_R
15      Save_dir_TOTG = Save_dirA_G + Save_dirB_G
16      Save_dir_TOTB = Save_dirA_B + Save_dirB_B
17
      with fits.open(Root_dir_TOT) as hdul:
20
21 #Use openCV to assign each colour to arrays of respective colours:
22          fits_data = hdul[0].data;
23          hdu = fits.PrimaryHDU()
24          hdr = hdul[0].header
25 #Use openCV to split the nd array into a tuple of 3 colours,
       interpolating to go from RGGB to RGB
26          fits_data_split = cv2.cvtColor(fits_data,cv2.COLOR_BayerRGGB2RGB)
27 #Use openCV to split the nd array into a tuple of 3 colours,
       interpolating to go from GRBG to RGB
28          #fits_data_split = cv2.cvtColor(fits_data,cv2.COLOR_BayerGRBG2RGB)
29          fds_R, fds_G, fds_B = cv2.split(fits_data_split)
30
31          #Create Red Image
32          hdu_R = fits.PrimaryHDU(fds_R)
33          print("hdu_R",hdu_R)
34          hdul_R = fits.HDUList([hdu_R])
35          hdul_R[0].header = hdr
36          hdr_R = hdul_R[0].header
37 #Add filter information to header section. - now 44 parameters
38          hdr_R['Filter'] = "TR"
39
40 #Write header and array information to file location
41          hdul_R.writeto(Save_dir_TOTR,overwrite = True)
42
43
44          #Create Green Image
45          hdu_G = fits.PrimaryHDU(fds_G)
46          hdul_G = fits.HDUList([hdu_G])
47          hdul_G[0].header = hdr
48          hdr_G = hdul_G[0].header
49          #Add filter information to header section. - now 44 parameters
50          hdr_G['Filter'] = "TG"
51
52          #Write header and array information to file location
53          hdul_G.writeto(Save_dir_TOTG,overwrite = True)
54
55
56          #Create Blue Image
57          hdu_B = fits.PrimaryHDU(fds_B)
58          hdul_B = fits.HDUList([hdu_B])
59          hdul_B[0].header = hdr
60          hdr_B = hdul_B[0].header
61          #Add filter information to header section. - now 44 parameters
62          hdr_B['Filter'] = "TB"
63
64          #Write header and array information to file location
65          hdul_B.writeto(Save_dir_TOTB,overwrite = True)
66
67
68          #check that the above has worked by calling one of the files
69          CHECKR = '/content/drive/MyDrive/Project/Debayer Code and
       Files/Dominique_Collection/TrES-3b_2021-08-29_ASI294C_RGGB_120s/
       Split_R/Flats_28aout_24ms_G121_T15_00005_1 IR Cut_Flat_R.fit'
70          REDDEB = fits.open(CHECKR)
71          print(hdr_R['DATE-OBS'])
```

```
72          fits.getdata(CHECKR,header=True)
```

Listing 2: Python Debayer Code for Flat Frames.

G.1.3 Python Duplication Code - Bias and Dark Frames

Dark and bias frames, due to containing only subtractive information where we intend to receive no light input on the sensor are constant across all colours as their effect is not wavelength dependant but induced by instrumental errors such as imperfections upon the telescope mirror. With this, automation of this process to rename and duplicate these files for analysis streamlines the observation process.

- Loop through Bias and Dark frames to duplicate files for each 'Split_X' folder.
- Construct file locations to access load and save locations for each colour channel.
- Loop through '.fits' to open file and copy information for Bias:
  - Set Header Data Unit, where HDUList represents the Primary for the file,
  - Create array of data without header information
  - Combine Primary Header Data Unit and array of information
  - Write file to three locations for each colour channel
- Loop through '.fits' to open file and copy information for Dark:
  - Set Header Data Unit, where HDUList represents the Primary for the file,
  - Create array of data without header information
  - Combine Primary Header Data Unit and array of information
  - Write file to three locations for each colour channel
- Load image data and Header Data Unit List information from save path to ensure all values represented and stored correctly in '.fits' format.

```
1 #Loop through Bias and Dark frames to duplicate files to Split_R,
      Split_G, Split_B folders
2 for num in range(1,8,1):
3       Root_dirA = '/content/drive/MyDrive/Project/Debayer Code and
      Files/Dominique_Collection / TrES -3 b_2022 -07 -11 _ASI2600 MC_RGGB_180
      s / Bias_100 pc_FZ_T 10_G 101_Off50_51 ms_2022 -05 -20 _FZ_1 x1__G 101_O 50_T -
      9.70 _E0
      -{:04 d}'.format(num)
4       Root_dirB = ".fits"
5       Root_dirB_TOT = Root_dirA + Root_dirB
6       Root_dirAD = '/content/drive/MyDrive/Project/Debayer Code and
      Files/Dominique_Collection / TrES -3 b_2022 -07 -11 _ASI2600 MC_RGGB_180 s /
      Darks_100 pc_180 sec_T 10_G 101_Off50 _2022 -05 -11 _FCLS_1 x1__G 101_O 50_T -
      9.60
      _E180 .00 s_{:04 d}'.format(num)
7
8       Root_dirD = ".fits"
9       Root_dirD_TOT = Root_dirAD + Root_dirD
10      #Root_dirA = '/content/drive/MyDrive/Project/Debayer Code and
      Files/Dominique_Collection / TrES -3 b_2021 -08 -29 _ASI294 C_RGGB_120
      s / Flats_28 aout_24 ms_G 121_T 15_{:04 d}'. format(num)
11
12      Save_dir_Rb = '/content/drive/MyDrive/Project/Debayer Code and
      Files/Dominique_Collection / TrES -3 b_2022 -07 -11 _ASI2600 MC_RGGB_180 s /
```

```
Split_R/Bias_100pc_FZ_T10_G101_Off50_51ms_2022-05-20_FZ_1x1__G101_O50
_T-9.70_E0
-{:04d}'.format(num)
 Save_dir_Gb = '/content/drive/MyDrive/Project/Debayer Code and
Files/Dominique_Collection/TrES-3b_2022-07-11_ASI2600MC_RGGB_180s/
Split_G/Bias_100pc_FZ_T10_G101_Off50_51ms_2022-05-20_FZ_1x1__G101_O50
_T-9.70_E0
-{:04d}'.format(num)

 Save_dir_Bb = '/content/drive/MyDrive/Project/Debayer Code and
Files/Dominique_Collection/TrES-3b_2022-07-11_ASI2600MC_RGGB_180s/
Split_B/Bias_100pc_FZ_T10_G101_Off50_51ms_2022-05-20_FZ_1x1__G101_O50
_T-9.70_E0
-{:04d}'.format(num)
 Save_dir_Rd = '/content/drive/MyDrive/Project/Debayer Code and
Files/Dominique_Collection/TrES-3b_2022-07-11_ASI2600MC_RGGB_180s/
Split_R/Darks_100pc_180sec_T10_G101_Off50_2022-05-11_FCLS_1x1__G101_O
50_T-9.60
_E180.00s_{:04d}'.format(num)
 Save_dir_Gd = '/content/drive/MyDrive/Project/Debayer Code and
Files/Dominique_Collection/TrES-3b_2022-07-11_ASI2600MC_RGGB_180s/
Split_G/Darks_100pc_180sec_T10_G101_Off50_2022-05-11_FCLS_1x1__G101_O
50_T-9.60
_E180.00s_{:04d}'.format(num)
 Save_dir_Bd = '/content/drive/MyDrive/Project/Debayer Code and
Files/Dominique_Collection/TrES-3b_2022-07-11_ASI2600MC_RGGB_180s/
Split_B/Darks_100pc_180sec_T10_G101_Off50_2022-05-11_FCLS_1x1__G101_O
50_T-9.60
_E180.00s_{:04d}'.format(num)


 Save_dir_TOTBR = Save_dir_Rb + Root_dirB
 Save_dir_TOTBG = Save_dir_Gb + Root_dirB
 Save_dir_TOTBB = Save_dir_Bb + Root_dirB

 Save_dir_TOTDR = Save_dir_Rd + Root_dirD
 Save_dir_TOTDG = Save_dir_Gd + Root_dirD
 Save_dir_TOTDB = Save_dir_Bd + Root_dirD

 with fits.open(Root_dirB_TOT) as hdul:
        #open fits file at root location [WILL BE IN LOOP]

        #set Header Data Unit, where hdul is often represents the
 primary for the fits file: type = <class 'astropy.io.fits.hdu.
 hdulist.HDUList'>
     fits_data = hdul[0].data;
        #numpy array of data, without any header information
     hdu = fits.PrimaryHDU(fits_data)
        #set primary Header Data unit, encapsulating the data for the
primary for fits file: type = <class 'astropy.io.fits.hdu.image.
PrimaryHDU'>
     hdr = hdul[0].header
        #full Header data as seen at the start of fits document, eg has
43 parameters
     hdulB = fits.HDUList([hdu])
     hdulB[0].header = hdr

     hdulB.writeto(Save_dir_TOTBR,overwrite = True)
        #Create and write header and array information to destination
path file
```

```
38          hdulB.writeto(Save_dir_TOTBG,overwrite = True)
39          hdulB.writeto(Save_dir_TOTBB,overwrite = True)
40
41
42      with fits.open(Root_dirD_TOT) as hdul:
                #open fits file at root location [WILL BE IN LOOP]
43
                #set Header Data Unit, where hdul is often represents the
        primary for the fits file: type = <class 'astropy.io.fits.hdu.
        hdulist.HDUList'>
44          fits_data = hdul[0].data;
                #numpy array of data, without any header information
45          hdu = fits.PrimaryHDU(fits_data)
#set primary Header Data unit, encapsulating the data for the

        primary for fits file: type = <class 'astropy.io.fits.hdu.image.
        PrimaryHDU'>
46          hdr = hdul[0].header
                #full Header data as seen at the start of fits document, eg has
        43 parameters
47          hdulB = fits.HDUList([hdu])
48          hdulB[0].header = hdr
49
50          hdulB.writeto(Save_dir_TOTDR,overwrite = True)
                #Create and write header and array information to destination
        path file
51          hdulB.writeto(Save_dir_TOTDG,overwrite = True)
52          hdulB.writeto(Save_dir_TOTDB,overwrite = True)
53
54  #Check the files are saved to the right location
55  CHECKR = '/content/drive/MyDrive/Project/Debayer Code and Files/HAT-P-54b/
        Split_R/Altair_Sky_Flat-0005 Flat_R.fit'
56  REDDEB = fits.open(CHECKR)
57  print( hdr['DATE - OBS'])
58  fits.getdata(CHECKR,header=True
```

Listing 3: Python Code for Bias and Dark Frames Duplication.